Bioinspiration &
Biomimetics

PURPOSE-LED
PUBLISHING™

Skin Deep: a novel biomimetic control strategy for rectilinear locomotion in snake robots

To cite this article before publication: Henry C. Astley 2026 *Bioinspir. Biomim.* in press https://doi.org/10.1088/1748-3190/ae73d6

IOP Publishing Journal Title
Journal **XX** (XXXX) XXXXXX https://doi.org/XXXX/XXXX

Skin Deep: a novel biomimetic control strategy for rectilinear locomotion in snake robots

Henry C. Astley[1*]

[1] Department of Biology, Biomimicry Research & Innovation Center, University of Akron, Akron, OH, USA

*Author to whom any correspondence should be addressed.

E-mail: hastley@uakron.edu

Received xxxxxx
Accepted for publication xxxxxx
Published xxxxxx

Abstract

Snakes are masters of movement through cluttered, confined, and complex habitats, leading to attempts to replicate this mastery in snake robots to improve our access to these challenging environments. While snakes use a variety of locomotor modes, rectilinear allows snakes to move through even the narrowest of spaces. However, while other modes are driven by axial bending, rectilinear relies on motion of the muscular skin, making it challenging to replicate in robots. Prior robotic rectilinear was achieved using secondary actuator systems (e.g. prismatic joints), anteriorly propagating waves, and/or standing waves, which require additional mechanical complexity, high vertical clearance, or dedicated parts for symmetry-breaking (e.g. electromagnets, deployable frictional pads), respectively. Here, I present a new algorithm which closely matches the robot to the motion of the snake's ventral skin (rather than the whole body) during rectilinear locomotion. Robot segments are assigned roles of either rigid ventral scales or flexible inter-scale skin. As in biological snakes, "scale segments" are lifted clear of the substrate and moved forward via contraction and expansion of the adjacent "skin motors". This "cutaneous rectilinear algorithm" allows rectilinear locomotion without the need for additional actuators or other specialized modifications, and achieves similar displacement per cycle and current consumption to propagating vertical wave methods at a lower vertical height, improving access to highly confined spaces.

Keywords: Snake, rectilinear, robotics

1. Introduction

To effectively traverse the natural world, animals have evolved myriad adaptations which allow them exceptional capabilities across challenging environments and intense mechanical demands [1–4]. The desire to replicate these remarkable feats has led to bioinspired robots which can swim, run, jump, climb and fly [5–9]. Such bioinspired robots often have surprising solutions of mechanical challenges, and can outperform traditional robots, particularly in challenging natural environments such as sand, unstructured terrain, and complex flows [7,10–15].

A common mechanical challenge is the need to move effectively through highly restricted and structurally complex environments, such as narrow pipes or densely cluttered structures, and for this application, snakes are an ideal model taxa [16–18]. The elongate body and highly diverse locomotor repertoire of snakes allows them to move rapidly and efficiently through environments which are difficult or impossible for other animals of equivalent mass. Indeed, their most recognizable form of locomotion, slithering, uses the environmental structures which are obstacles to limbed animals as propulsive 'push points' [19,20], allowing them to increase their speed as obstacle density increases (up to a limit) [21] while limbed species must slow down [11,22–25]. Unlike limbed species, which shift locomotor mode primarily

based on speed (e.g. walk to trot to gallop) [26,27], snakes shift locomotor mode based on substrate mechanics and geometry [20,28–30], with over 20 described modes for environments ranging from loose desert sand to large tree branches to narrow tunnels [30].

Of crucial relevance to snake robots, rectilinear locomotion (Figure 1) is often used to move through spaces only slightly larger than the snake's body [31–33]. Rectilinear locomotion is most easily elicited in heavy bodied vipers, pythons, and boas, but is present in nearly all snakes as well as Amphisbaenian lizards (limbless except for genus *Bipes*) [34]. Unlike other modes of locomotion which are powered by bending of the vertebral column, rectilinear locomotion is powered by motions of the skin alone (Figure 1), with no need for axial bending aside from turning [30–34]. During this mode, the enlarged ventral scales are pulled upwards and forwards relative to the ribs (which are held static or largely so) and the ground, stretching the skin posterior to the scale and contracting the skin anterior to it (Figure 1) [30–35]; this mode seems to function whether the moving scale is fully lifted clear of the substrate or simply subject to lower pressure allowing easier sliding [32,33]. The large ventral scale then makes firm static contact with the ground again, anchoring via friction as the skeleton and body are pulled forward over the snake, resulting in contraction of the posterior skin and stretching of the anterior skin (Figure 1) [30–34]. These motions are repeated slightly out of phase in a posteriorly-propagating wave, resulting in multiple propagating regions of movement and stasis of the ventral skin along the body (Figure 1) [30–34]. For a detailed examination of the kinematics, anatomy, and muscle activity, see [33].

For replication of rectilinear locomotion in bioinspired robots, the two crucial mechanical events are 1) the fore-aft motions of the ventral scales and 2) the ability to control contact forces (Figure 1) [31,33]. While in biological snakes, the expansion and contraction of the skin is largely driven by extrinsic muscles connecting to the ribs (the costocutaneous superior and inferior) [31,33], the underlying physical principle is that the contact points are cyclically and forcefully displaced to produce net motion relative to the overall body. Robotic mechanisms to achieve this displacement are varied but generally fall into two categories – axial actuators and vertical bending [36–39]. Axial actuators include any actuation mechanism which increases and decreases the distance between adjacent robot segments, such as prismatic or leadscrew mechanisms with electric motors, pneumatics, electroactive polymers, etc. [36–38,40–43]; many such mechanisms could also be considered analogous to earthworms [44,45]. Vertical bending can take the form of either standing waves which oscillate in amplitude (as in an inchworm caterpillar) [36,46–51], or anteriorly-propagating waves[36,39,52–54], both using revolute joints across successive segments, as seen in many snake robots performing other locomotor modes [16,55,56]. While standing wave methods use amplitude changes of the standing wave to cyclically change the distance between the first and last segment, anteriorly-propagating waves use the discrepancy between path length of the body and distance between ground contact points to achieve forward displacement [36]. This last method is capable of quite high speeds [39,53,54,57], but requires substantial vertical height changes to do so. Regardless of the mechanism used to displace contact points, effective forward motion requires some method of controlling contact point traction force, otherwise the robot will simply move in place with no net forward motion[36]. These can be in the form of directly actuated mechanisms such as grippers[40], electromagnets [46,47,51], shifting mass [48], or friction control via deployable frictional pads [37], ratcheting wheels [50], directional asymmetry in friction (passively or actively) [42,43,49], or simple lifting and lowering to make and break contact (as in the anteriorly-propagating waves) [36,41].

As part of the extraordinary success of snakes in moving through cluttered, confined, and complex environments

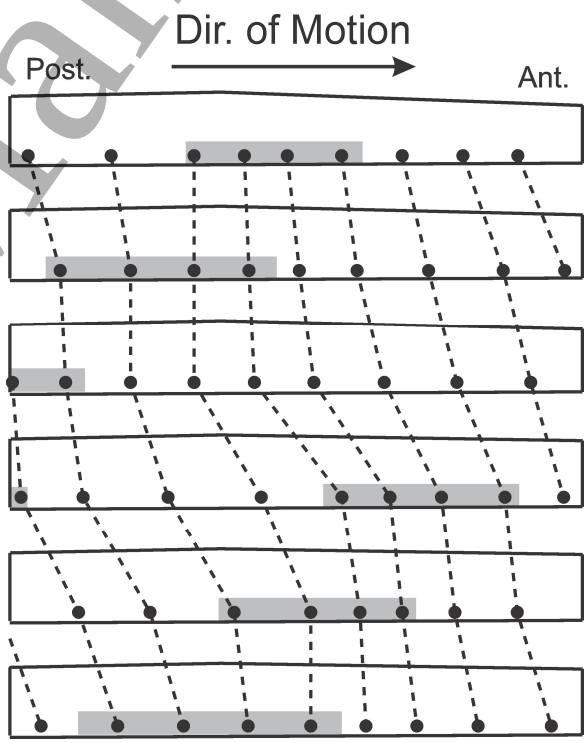

Figure 1. Diagram of rectilinear locomotion in snakes, showing a lateral view of a body segment. Points on the body are black dots, with dashed lines connecting the points over time (vertically downwards) to show motion. Regions of scales and skin are lifted and moved anteriorly, then lowered and placed into static contact with the ground (grey); posterior muscular force on the scales results in forward motion of the body. Image from [18], modified via Creative Commons.

derives from their diversity of locomotor modes, an effective snake robot will ideally be able to implement multiple modes simultaneously [17,18]. While a robot consisting of alternating vertical and horizontal motors can easily be programmed to produce sidewinding [58–60], lateral undulation [16,61], and tunnel concertina locomotion [62,63], rectilinear locomotion remains a challenge without secondary mechanisms as described above. The addition of axial actuators increases mechanical complexity and weight, as does the addition of actively controlled mechanisms to regulate contact, and asymmetric friction is often contingent upon the substrate properties. While an anteriorly propagating wave does not require additional mechanical complexity, it does require greater changes in vertical height than axial actuator methods, which is counter to the role of rectilinear locomotion (and snake robots more broadly) in navigation of highly enclosed spaces.

I propose a new control algorithm, termed the "Cutaneous Rectilinear Algorithm", based on close replication of the scale and skin motions observed in live snakes during rectilinear locomotion. This new algorithm allows any snake robot with vertical bending capability to achieve rectilinear locomotion, without the need for additional mechanisms or modifications. I hypothesize that the Cutaneous Rectilinear Algorithm will show comparable displacement per cycle to the vertical undulation algorithm, and while maintaining low vertical height and current consumption.

2. Methods

2.1 Cutaneous Rectilinear Algorithm

The cutaneous rectilinear algorithm's fundamental premise is to assign fixed identities to individual regions of the robot as either ventral scales (henceforth "Scales") or inter-scale skin (henceforth "Skin") (Figure 2A-E, Sup. Vids. 1 & 2). Scales consist of a single segment, while Skin regions consist of two or more segments in series and all motors connected to them (including those connected to the adjacent Scales) (Figure 2A-E, Sup. Vids. 1 & 2). In this paper, I tested versions of this algorithm with two and three segments in the Skin region, henceforth termed "triangular" and "rectangular", respectively, based on the shape when maximally contracted (Figure 2AG, Sup. Vids. 1 & 2). The first and last segments are Scale segments, with at least one additional Scale segment in between (two or three in this paper's implementation) (Figure 2A-E, Sup. Vids. 1 & 2). At the start of the cycle, all Scales are flat against the ground, and all Skin regions are maximally contracted except for the first, which is extended, with the segments straight and flat against the ground (Figure 2A, Sup. Vids. 1 & 2).

The procedure to move a Scale segment consists of three stages: Lifting, Scale Movement, and Lowering.

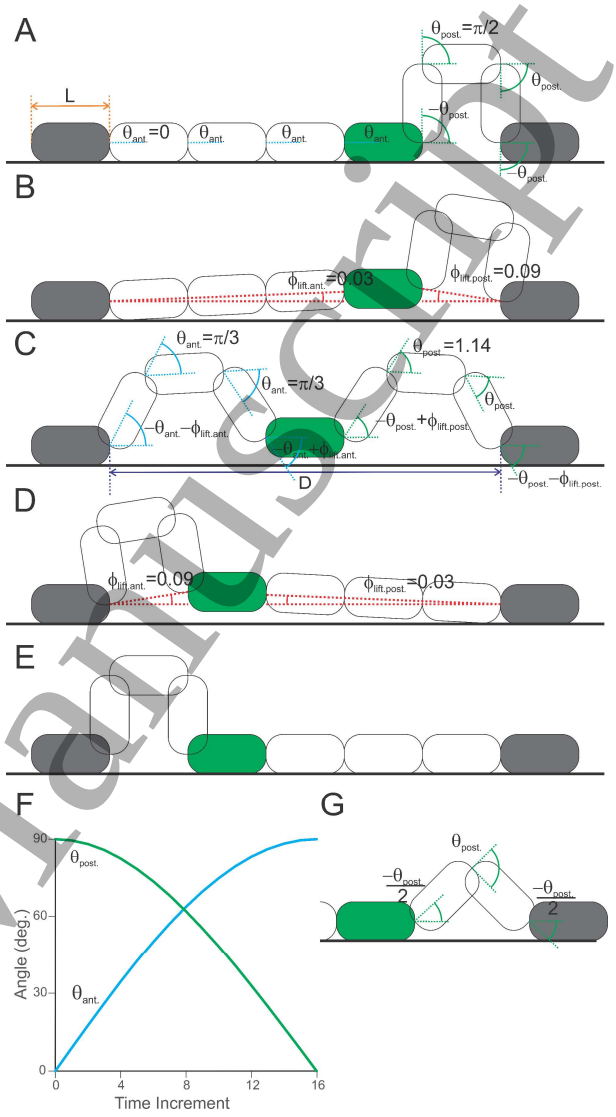

Figure 2. Control of the Cutaneous Rectilinear Algorithm in an example snake robot, moving towards the left. Static "Scale" segments are grey, the moving "Scale" segment is green, and "Skin" segments are white. Segment length (L) is shown in A, while the length of the moving region (D) is shown in C. A) Initial Position, using "rectangular" variation (3 motors in "Skin" segments). B) The moving scale is lifted clear of the ground. C) Synchronous contraction of the anterior "Skin" region and extension of the posterior "Skin" region translate the lifted "Scale" forward, while it remains lifted. D) Conclusion of motion. E) The lifting offsets are returned to zero. The cycle can now repeat for the most posterior segment. F) Angle change over 16 time increments for skin motors to ensure smooth motion. G) Alternate angles for "triangular" variation using 2 "Skin" motors.

2.1.1 Lifting. First, the moving Scale is lifted above the ground by tilting the adjacent Skin regions (Figure 2B, Sup. Vids. 1 & 2). For the anterior Skin region, the anterior motor

is dorsiflexed while the posterior motor is ventroflexed, while this is reversed in the posterior Skin region (Figure 2B, Sup. Vids. 1 & 2). Because the anterior Skin region is longer than the posterior one, imposing the same motor angle for lift in both resulting in poor contact and slipping. To mitigate this, the angle of lifting was adjusted via the law of sines, which showed that the ratio between the sines of the lifting angles for the anterior and posterior Skin regions was proportional to the ratio between the lengths of the anterior and posterior Skin regions. Since a peak of 5° of lifting was sufficient for ground clearance of the moving Scale, the small angle approximation allowed simplifying the ratio of sines to the ratio of angles (Figure 2B). The initial lifting angle was 5° for the posterior Skin segment, with the anterior Skin segment angle calculated as above; this was recalculated through the subsequent commands during the second stage, with the anterior Skin segment being lifted at 5° at the end (Figure 2D).

2.1.2 Scale Movement. Second, the anterior Skin region is contracted while the posterior Skin region is lengthened (Figure 2BCD, Sup. Vids. 1 & 2). In order to prevent slipping at the adjacent static Scale segments, these changes had to be matched such that the total distance between static Scale segments (D) is constant. For a version with 3 segments and 4 motors in the Skin region ("rectangular"), the middle two motors will always be at equal angles while the outer two will be at that same angle in the opposite direction (aside from a pair of slight offsets to preserve lifting), thus each Skin region can be represented as a single angle, represented as q_{Ant} and q_{Post} (Figure 2B). As we can neglect the small effect of lifting via the small angle approximation, the total distance between static Scale segments (D) for a robot with segment length L can be expressed as

$$D = 2L\cos\theta_{Ant} + 3L + 2L\cos\theta_{Post}$$

For an initial position with $\theta_{Ant}=0$ and $\theta_{Post}=\pi/2$, D=5L and thus the relationship between θ_{Ant} and θ_{Post} must be

$$1 = \cos\theta_{Ant} + \cos\theta_{Post}$$

When using a 2 segment, 3 motor Skin region ("triangular") (Figure 2G), we designate the middle motor of each Skin region as the defining angle of the region, with the anterior and posterior motors being half of this value, thus

$$D = 2L\cos\frac{\theta_{Ant}}{2} + L + 2L\cos\frac{\theta_{Post}}{2}$$

For an initial position with $\theta_{Ant}=0$ and $\theta_{Post}=\pi/2$, D=3L + L$\sqrt{2}$ ≈ 4.414L and thus the relationship between θ_{Ant} and θ_{Post} must be

$$1 + \frac{\sqrt{2}}{2} = \cos\frac{\theta_{Ant}}{2} + \cos\frac{\theta_{Post}}{2}$$

To actuate the robot, θ_{Ant} was defined, with θ_{Post} computed according to the equations above. Initially q_{Ant} was computed via

$$\left[0, \frac{\pi}{2}\right] = \{i \in \mathbb{Z} | 0 \le i \le 16\}$$

$$\theta_{Ant} = i * \frac{\pi}{32}$$

However, when θ_{Ant} was changed linearly across its range, the arccosine necessary to compute θ_{Post} resulted in changes in q_{Post} below the resolution of the motors at the start of the motion and excessively rapid movement of θ_{Post} at the end of the motion, leading to slip and other abnormal motor behaviors. More specifically, at the start of motion, a change in θ_{Ant} from 0 to $\pi/32$ would only produce a change of ~$\pi/300$ in θ_{Post}, corresponding to only two increments in the motor command position, while the final change in θ_{Ant} from $15\pi/32$ to $\pi/2$ would produce a change of ~$\pi/6$ in θ_{Post}, corresponding to a 170-fold increase in motor speed. Thus, to produce smoother motion and lower slip, θ_{Ant} was computed

$$\theta_{Ant} = \frac{\pi}{2}\sin\left(\frac{i * \pi}{32}\right)$$

This resulted in calculated values of θ_{Post} similar to (but not identical to) a cosine (Figure 2F), which were more amenable to motor control. At the end of the motion, the anterior Skin region was maximally contracted, while the posterior Skin region was maximally extended (Figure 2D, Sup. Vids. 1 & 2).

2.1.3 Lowering. Finally, the lifting behavior was reversed, removing the offsets indicated previously and resulting in the moving Scale being laid flat against the ground, along with the posterior Skin region (Figure 2DE, Sup. Vids. 1 & 2).

2.1.4 Subsequent Scale Movements. This behavior was then replicated for the next posterior Scale segment, with the now-extended Skin region becoming anterior and a new, contracted Skin region becoming posterior (Sup. Vids. 1 & 2). This was repeated for all scales, including the last one, which resulted in lifting both the first and last Scale segments as the most posterior skin region contracts and the most anterior Skin region extends, restoring the initial position (Sup. Vids. 1 & 2).

2.1 Implementation & Testing

To test the cutaneous rectilinear algorithm's efficacy and compare it to alternatives, I used a snake robot consisting of 12 Dynamixel XL330-M288-T motors (ROBOTIS, Inc., South Korea) connected via custom 3D printed brackets, with an inert 3D printed segment serving as the anterior-most segment. This robot was placed such that all motors axes were horizontal and produced vertical bending. The robot was controlled using an OpenRB-150 controller (ROBOTIS, Inc., South Korea) running with Dynamixel2Arduino library 0.7.0 (ROBOTIS, Inc., South Korea) and powered via a 6V 2A DC power source. Code is included in supplementary material.

We compared five rectilinear control algorithms which can be implemented without additional actuators or

friction/contact manipulation. These included the "rectangular" and "triangular" variations of the cutaneous rectilinear algorithm and three versions of the vertical undulation algorithm (Sup. Vids. 3-5); the maximum motor angle allowed by the robot joints was slightly more than 90°, thus the maximum angle was set to 90° for both cutaneous rectilinear algorithms (Figure 2AG), with vertical wave maximum amplitudes of 90°, 60°, and 30°. Each of the vertical undulation versions had two complete waves on the body to always ensure at least two ground contact points, and differed only in maximum motor bending (30°, 60°, and 90°) (Sup. Vids. 3-5) [36,39,52–54]. While slightly higher values of maximum bending (100°) were mechanically possible without self-intersection, these values caused the robot to topple to the side within a cycle, and were not tested.

The snake robot was placed on a smooth, level sheet of expanded PVC for trials. Each control algorithm was tested in five trials, with each trial consisting of five cycles of motion. To quantify performance, here defined as distance moved per cycle, I attached two round, IR-reflective markers to the most anterior segment, and quantified the motions of these markers using a system of eight Flex13 infrared motion tracking cameras at 120 fps, connected to and controlled via Optitrack Motive software (NaturalPoint, Inc., Corvallis, OR, USA). These cameras recorded the 3D position of the markers with sub-millimeter precision.

To assess energetics, I used the internal current sensing capabilities of the Dynamixel motors, which summed current consumption across all motors for each cycle and exported it via serial connection. We measured the current consumed when the robot was static, and total current when moving, as

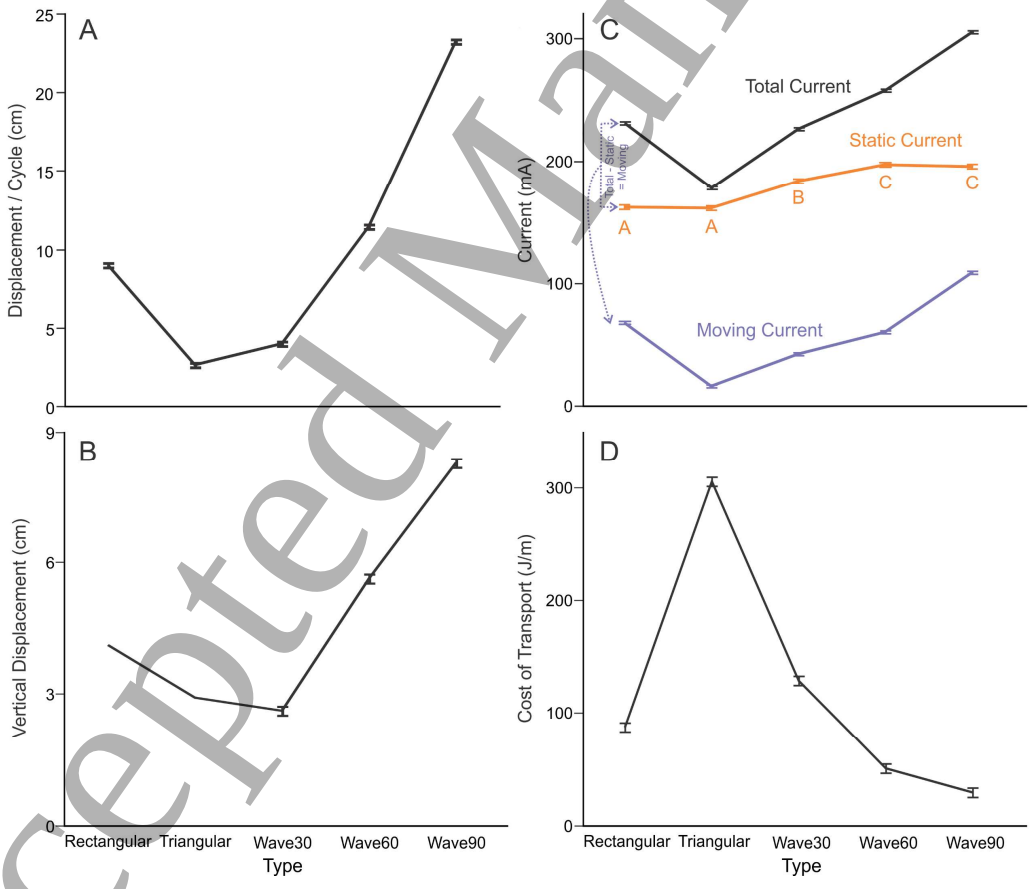

Figure 3. A) Displacement per cycle, B) Vertical displacement during a cycle, C) Current consumption, showing total average current per cycle, current while maintaining a static posture, and moving current (= total - static), and D) Cost of Transport. All pairwise differences were significant except for static current, with letters showing the results of Tukey's Honest Significant Differences. Error bars are omitted from cutaneous rectilinear algorithm vertical displacements, as these were measured from static height.

well as the difference between the moving current and the mean static current of a given algorithm (to reduce extraneous variability). By separating these components out, I can distinguish the cost of maintaining a given posture, particularly one in which segments are actively elevated above the ground, from the actual cost of forward movement; this distinction is inspired by measurements of the energetics of terrestrial animal locomotion, which distinguishes the cost of movement (Net Cost of Transport, J per kg per meter) from the cost of stance and basal metabolic rate [64]. Cost of Transport (in Joules per meter) was calculated as the total current multiplied by the voltage (5V) and cycle duration, divided by distance per cycle.

Finally, height was assessed by measuring the maximum vertical displacement during locomotion from the motion capture data for anteriorly-propagating waves. Because the most anterior segment did not elevate during the new rectilinear algorithm, vertical height was calculated from motor and bracket geometry and confirmed via static measurement. To confirm the ability of the rectanular algorithm to negotiate a tunnel lower than the quantified width, an additional video was recorded demonstrating this behavior in a tunnel of 7.5 cm height, constructed of the same expanded PVC material as the floor of the original test arena (Sup. Vid. 6).

All variables were compared using a single factor ANOVA with control algorithm as a fixed factor, and pairwise differences for significant effects assessed using Tukey's HSD.

3. Results

The cutaneous rectilinear algorithm achieved successful locomotion, defined as positive displacement per cycle for five continuous cycles (Figure 3A, Sup. Vids. 1 & 2). The "triangular" implementation achieved similar but slightly lower displacement to the 30° vertical wave, and the "rectangular" implementation achieved similar but slightly lower displacement to the 60° vertical wave; the 90° vertical wave achieved the highest displacement per cycle (Figure 3A). All differences were statistically significant ($F_{4,120}$=13298, $p<0.0001$), and all pairwise comparisons were different.

Current consumption was also different across algorithms, with all current variables showing main effects ($F_{4,120}$=339, $p<0.0001$); all pairwise comparisons were different except for static current consumption, in which differences are denoted by letter (Figure 3C). Static current consumption was highest for high-amplitude vertical waves, lowest for the cutaneous rectilinear algorithm, and intermediate for the 30° vertical wave (Figure 3C). Total current consumption and differential current consumption (total-static) were both significantly different across algorithms (Total Current: $F_{4,120}$=5772, $p<0.0001$, Differential Current: $F_{4,120}$=3163, $p<0.0001$); all pairwise comparisons were significantly different. Current consumption increased with vertical wave amplitude and was higher in the rectangular than triangular cutaneous rectilinear algorithm (Figure 3C). In all cases, the triangular rectilinear algorithm was cheapest, with the rectangular rectilinear algorithm being similar but slightly more costly than the 30° vertical wave for total current consumption and the 60° vertical wave for differential current consumption (Figure 3C). When expressed in terms of energy consumed per meter moved, all algorithms were significantly different ($F_{4,120}$=2889, $p<0.0001$). Increasing vertical wave amplitude reduced cost of transport, and the rectangular cutaneous rectilinear algorithm was substantially lower cost than the triangular version, as well as being lower than the 30° vertical wave (Figure 3D).

Both versions of the cutaneous rectilinear algorithm were substantially lower in height than the 60° and 90° vertical waves (Figure 3B). The triangular version was slightly taller than the 30° vertical wave, while the 90° vertical wave was far taller than other algorithm (Figure 3A).

4. Discussion

This paper demonstrates the proposed novel bio-inspired algorithm for snake robot rectilinear locomotion is effective (Sup. Vids. 1 & 2), and capable of achieving comparable locomotor performance to anteriorly propagating wave algorithms with similar or lower current cost for comparable performance and substantially lower vertical height (Figure 3B). As a key purpose of snake-inspired robots is to access confined environments [16–18], this represents a significant advantage; the only situation in which rectilinear would be necessary but high-amplitude vertical wave algorithms would be superior is strongly laterally confined but vertically tall or unconfined environments. For extreme vertical height limitations, both the triangular version of the cutaneous rectilinear algorithm and the 30° vertical wave algorithm were similar in overall performance (Figure 3AB).

The relationship between displacement per cycle, vertical height, and motor parameters is a key difference between these algorithms (Figure 3A). For vertical waves, vertical height and displacement per cycle are causally linked (Figure 3A), and the relationship is largely independent of the motor number or their range of motion (provided they are sufficient to realize the commanded waveform). As the wave becomes higher amplitude, displacement and vertical amplitude both increase until a limit caused by geometric intersection of the waves; this intersection occurs well below the limits of the range of motion of the motors. Motor geometry affects this mode only insofar as it leads to toppling risk, with a narrower base reducing stability; this was observed directly in the slight deviations from a straight path in the 90° vertical wave (Sup. Vid. 5) and the toppling failures which prevented tests at

higher amplitudes. However, in a laterally confined space, this may be irrelevant. In contrast, the cutaneous rectilinear algorithm is strongly influenced by the number of motors and their ranges of motion, as evidenced by the difference in performance between the rectangular and triangular versions (Figure 3A). The fundamental mechanism of displacement in the cutaneous rectilinear algorithm relies upon the differnce in length between the expanded and contracted Skin region (Figure 2A-E), hence why the rectantular version (Extended Skin Region Length = 3L, Contracted Skin Region Length = 2L) outperforms the triangular version (Extended = 2L, Contracted = $2L*\cos(\pi/4)=2*L*0.707$). Increased number of motors would improve performance by allowing more complex geometries of the "skin" segments both when maximally shortened and during the geometric changes from shortened to elongated or vice versa, but with a tradeoffs of vertical height; if motors remained limited to a maximum angle of 90°, a Skin Region comprised of 6 segments and 7 motors in the shape of an Ω could theoretically exceed the displacement of the 90° vertical wave, but at the cost of greater vertical height. In contrast, increasing the motor range of motion could increase displacement per cycle without tradeoffs between displacement and vertical height, particularly in combination with increased number of segments in each Skin region; with a 180° range of motion, a Skin Region of N segments could achieve a displacement of N * segment length while never exceeding a height of the segment length. Additional motors may also allow multiple moving scales at once, as in biological snakes (Figure 1) [31,33,35]. Finally, the dramatic reduction in cost of transport between rectangular and triangular version of the cutaneous rectilinear algorithm suggests that future improvements may be able to achieve still greater energy savings. As such, the difference between these algorithms goes beyond the performance differences of these particular implementations, but in the scope of possible future innovations: the simplicity of vertical wave rectilinear offers easy control and high performance but little opportunity for future improvement, while the range of design space for the Cutaneous Rectilinear Algorithm is far greater than the two versions implemented here, particularly with corresponding hardware improvements.

This paper compares only two of the many known implementations of rectilinear locomotion (or similar movements) in snake-inspired robots [36,37,39,41,46,49]. As explained above, these other implementations often rely on fundamentally different mechanisms, making direct comparisons meaningless, and require additional mechanical complexity. "Inchworm" style robots [36,47–49,65] deserve special mention, as the cutaneous rectilinear algorithm could simply be thought of as two or more of such robots joined together and carefully coordinated. However, these standing-wave mechanisms require a method to break symmetry in order to achieve forward motion. While most such robots do so via dedicated secondary mechanisms or surfaces with anisotropic friction, the lifting and lowering of the middle "Scale" segments to regulate contact (Figure 2A-E) serves to break symmetry in the cutaneous rectilinear algorithm, allowing it to be implemented on any snake robot comprised of a series of servomotors capable of vertical motion, without further additions (Figure 2A-E, Sup. Vids. 1 & 2). Furthermore, by controlling contacts to maintain static posture at all ground contact points, this method should be less sensitive to terrain friction, and the algorithm could be easily modified to accommodate vertical unevenness in the terrain by simply increasing lifting height and biasing the anterior and posterior lifting angles. A snake robot comprised only of vertical and lateral bending motors (e.g. alternating servomotors) could be programmed to perform sidewinding [58–60], slithering (either planar or with both lateral and vertical combinations) [16,61,66], concertina [62,63], and rectilinear locomotion, the four key "categories" of snake locomotion (problematic as such categorization is, see [30]). This locomotor versatility is key to the success of snakes and will move bio-inspired snake robots incrementally closer to replicating their remarkable locomotor capabilities.

Acknowledgements

This work was supported by NSF BIO IOS Award #2045581 to HCA.

References

[1] Hildebrand M. Functional Vertebrate Morphology. Cambridge, Mass.: Belknap Press of Harvard University Press; 1985.

[2] Nussbaum MC. Aristotle's De Motu Animalium: Text with Translation, Commentary, and Interpretive Essays. Princeton University Press; 1985. https://doi.org/10.2307/2025643.

[3] Biewener AA. Animal Locomotion. New York: Oxford University Press; 2003.

[4] Vogel S. Comparative Biomechanics: Life's Physical World. Princeton: Princeton University Press; 2003.

[5] Ayers J, Witting J. Biomimetic approaches to the control of underwater walking machines. Philosophical Transactions of the Royal Society A: Mathematical, Physical and Engineering Sciences 2007;365:273.

[6] Lauder GV, Anderson EJ, Tangorra J, Madden PGA. Fish biorobotics: kinematics and hydrodynamics of self-propulsion. The Journal of

Experimental Biology 2007;210:2767–80. https://doi.org/10.1242/jeb.000265.

[7] Benyus JM. Biomimicry : innovation inspired by nature. HarperCollins e-books; 2009.

[8] Flammang BE. Bioinspired Design in Research: Evolution as Beta-Testing. Integrative and Comparative Biology 2022;62:1164–73. https://doi.org/10.1093/icb/icac134.

[9] Ishida M, Berio F, Di Santo V, Shubin NH, Iida F. Paleoinspired robotics as an experimental approach to the history of life. Science Robotics 2024;9:eadn1125. https://doi.org/10.1126/scirobotics.adn1125.

[10] Daley MA, Usherwood JR, Felix G, Biewener AA. Running over rough terrain: guinea fowl maintain dynamic stability despite a large unexpected change in substrate height. Journal of Experimental Biology 2006;209:171–87.

[11] Sponberg S, Full RJ. Neuromechanical response of musculo-skeletal structures in cockroaches during rapid running on rough terrain. Journal of Experimental Biology 2008;211:433.

[12] Mazouchova N, Gravish N, Savu A, Goldman DI. Utilization of granular solidification during terrestrial locomotion of hatchling sea turtles. Biology Letters 2010;6:398–401. https://doi.org/10.1098/rsbl.2009.1041.

[13] Li C, Hsieh ST, Goldman DI. Multi-functional foot use during running in the zebra-tailed lizard (Callisaurus draconoides). Journal of Experimental Biology 2012;215:3293–308. https://doi.org/10.1242/jeb.061937.

[14] Sefati S, Neveln ID, Roth E, Mitchell TRT, Snyder JB, MacIver MA, et al. Mutually opposing forces during locomotion can eliminate the tradeoff between maneuverability and stability. Proceedings of the National Academy of Sciences 2013;110:18798–803.

[15] Karakasiliotis K, Thandiackal R, Melo K, Horvat T, Mahabadi NK, Tsitkov S, et al. From cineradiography to biorobots: an approach for designing robots to emulate and study animal locomotion. Journal of the Royal Society Interface 2016;13.

[16] Hirose S. Biologically inspired robots : snake-like locomotors and manipulators. Oxford University Press; 1993.

[17] Astley HC. Slithering Across Worlds – Snake-Inspired Robots for Extraterrestrial Exploration. In: Eggermont M, Shyam V, Hepp A, editors. Biomimetics in Aerospace, 2022.

[18] Tingle JL, Garner KL, Astley HC. Functional diversity of snake locomotor behaviors: A review of the biological literature for bioinspiration. Annals of the New York Academy of Sciences 2024;n/a. https://doi.org/10.1111/nyas.15109.

[19] Gray J, Lissmann HW. The kinetics of locomotion of the grass snake. Journal of Experimental Biology 1950;94:15–42.

[20] Jayne BC. Kinematics of terrestrial snake locomotion. Copeia 1986;1986:195–208.

[21] Kelley KC, Arnold SJ, Gladstone J. The effects of substrate and vertebral number on locomotion in the garter snake Thamnophis elegans. Functional Ecology 1997;11:189–98.

[22] Collins CE, Self JD, Anderson RA, McBrayer LD. Rock-dwelling lizards exhibit less sensitivity of sprint speed to increases in substrate rugosity. Zoology 2013;116:151–8. https://doi.org/10.1016/J.ZOOL.2013.01.001.

[23] Parker SE, McBrayer LD. The effects of multiple obstacles on the locomotor behavior and performance of a terrestrial lizard. The Journal of Experimental Biology 2016;219:1004–13. https://doi.org/10.1242/jeb.120451.

[24] Gast K, Kram R, Riemer R. Preferred walking speed on rough terrain: is it all about energetics? The Journal of Experimental Biology 2019;222:jeb185447. https://doi.org/10.1242/jeb.185447.

[25] Clifton GT, Holway D, Gravish N. Uneven substrates constrain walking speed in ants through modulation of stride frequency more than stride length. Royal Society Open Science 2020;7:192068. https://doi.org/10.1098/rsos.192068.

[26] Hoyt DF, Taylor RC. Gait and the energetics of locomotion in horses. Nature 1981;292:239–40.

[27] Hildebrand M. Walking and running. In: Hildebrand M, Bramble DM, Liem KF, Wake DB, editors. Functional vertebrate morphology, Cambridge Massachusetts: Belknap Press of Harvard University Press; 1985, p. 38–57.

[28] Mosauer W. On the locomotion of snakes. Science 1932;76:583–5.

[29] Gray J. The mechanism of locomotion in snakes. Journal of Experimental Biology 1946;23:101–20.

[30] Jayne BC. What Defines Different Modes of Snake Locomotion? Integrative and Comparative Biology 2020. https://doi.org/10.1093/icb/icaa017.

[31] Lissmann HW. Rectilinear Locomotion in a Snake (Boa Occidentalis). Journal of Experimental Biology 1950;26:368–79.

[32] Marvi H, Bridges J, Hu DL. Snakes mimic earthworms: propulsion using rectilinear travelling waves. Journal of the Royal Society Interface 2013;10. https://doi.org/10.1098/rsif.2013.0188.

[33] Newman SJ, Jayne BC. Crawling without wiggling: muscular mechanisms and kinematics of rectilinear locomotion in boa constrictors. The Journal of Experimental Biology 2018;221:jeb.166199. https://doi.org/10.1242/jeb.166199.

[34] Gans C. Tetrapod limblessness: evolution and functional corollaries. American Zoologist 1975;15:455–67.

[35] Petersen JC, Jayne BC, Wilde AD, Capano JG, Roberts TJ. Effects of ingesting large prey on the kinematics of rectilinear locomotion in Boa constrictor. J Exp Biol 2024;227:jeb247042. https://doi.org/10.1242/jeb.247042.

[36] Chirikjian GS, Burdick JW. The kinematics of hyper-redundant robot locomotion. IEEE Transactions on Robotics and Automation 1995;11:781–93. https://doi.org/10.1109/70.478426.

[37] Hopkins JK, Gupta SK. Design and Modeling of a New Drive System and Exaggerated Rectilinear-Gait for a Snake-Inspired Robot. Journal of Mechanisms and Robotics 2014;6. https://doi.org/10.1115/1.4025750.

[38] Tang W, Reyes F, Ma S. Study on rectilinear locomotion based on a snake robot with passive anchor. 2015 IEEE/RSJ International Conference on Intelligent Robots and Systems (IROS), 2015, p. 950–5. https://doi.org/10.1109/IROS.2015.7353485.

[39] Zarrouk D, Mann M, Degani N, Yehuda T, Jarbi N, Hess A. Single actuator wave-like robot (SAW): design, modeling, and experiments*. Bioinspir Biomim 2016;11:046004. https://doi.org/10.1088/1748-3190/11/4/046004.

[40] Chen I-M, Yeo SH, Gao Y. Locomotive gait generation for inchworm-like robots using finite state approach. Robotica 2001;19:535–42. https://doi.org/10.1017/S0263574700003271.

[41] Primerano R, Pietrocola A, Janko M. A snake-like robot incorporating translational and rotation degrees of freedom. 2013 IEEE/RSJ International Conference on Intelligent Robots and Systems, 2013, p. 3279–84. https://doi.org/10.1109/IROS.2013.6696822.

[42] Saab W, Racioppo P, Kumar A, Ben-Tzvi P. Design of a miniature modular inchworm robot with an anisotropic friction skin. Robotica 2019;37:521–38. https://doi.org/10.1017/S0263574718001157.

[43] Marvi H, Meyers G, Russell G, Hu DL. Scalybot: A Snake-Inspired Robot With Active Control of Friction. ASME 2011 Dynamic Systems and Control Conference and Bath/ASME Symposium on Fluid Power and Motion Control, Volume 2, ASME; 2011, p. 443–50. https://doi.org/10.1115/DSCC2011-6174.

[44] Garrey WE, Moore AR. Peristalsis and coordination in the earthworm. American Journal of Physiology-Legacy Content 1915;39:139–48. https://doi.org/10.1152/ajplegacy.1915.39.2.139.

[45] Quillin KJ. Kinematic scaling of locomotion by hydrostatic animals: ontogeny of peristaltic crawling by the earthworm Lumbricus terrestris. J Exp Biol 1999;202:661–74. https://doi.org/10.1242/jeb.202.6.661.

[46] Kotay KD, Rus DL. Navigating 3D steel web structures with an inchworm robot. Proceedings of IEEE/RSJ International Conference on Intelligent Robots and Systems. IROS '96, vol. 1, 1996, p. 368–75 vol.1. https://doi.org/10.1109/IROS.1996.570701.

[47] Kotay K, Rus D. The Inchworm Robot: A Multi-Functional System. Autonomous Robots 2000;8:53–69. https://doi.org/10.1023/A:1008940918825.

[48] Rincon DM, Sotelo J. Ver-vite: dynamic and experimental analysis for inchwormlike biomimetic robots. IEEE Robotics & Automation Magazine 2003;10:53–7. https://doi.org/10.1109/MRA.2003.1256298.

[49] Serrano MM, Chang AH, Zhang G, Vela PA. Incorporating frictional anisotropy in the design

of a robotic snake through the exploitation of scales. 2015 IEEE International Conference on Robotics and Automation (ICRA), 2015, p. 3729–34. https://doi.org/10.1109/ICRA.2015.7139717.

[50] Shi Z, Pan J, Tian J, Huang H, Jiang Y, Zeng S. An Inchworm-inspired Crawling Robot. J Bionic Eng 2019;16:582–92. https://doi.org/10.1007/s42235-019-0047-y.

[51] Khan MB, Chuthong T, Danh Do C, Thor M, Billeschou P, Larsen JC, et al. iCrawl: An Inchworm-Inspired Crawling Robot. IEEE Access 2020;8:200655–68. https://doi.org/10.1109/ACCESS.2020.3035871.

[52] Akbarzadeh A, Kalani H. Design and Modeling of a Snake Robot Based on Worm-Like Locomotion. Advanced Robotics 2012;26:537–60. https://doi.org/10.1163/156855311X617498.

[53] Chang AH, Serrano MM, Vela PA. Shape-centric modeling of traveling wave rectilinear locomotion for snake-like robots. 2016 IEEE 55th Conference on Decision and Control (CDC), 2016, p. 7535–41. https://doi.org/10.1109/CDC.2016.7799433.

[54] Virgala I, Kelemen M, Prada E, Sukop M, Kot T, Bobovský Z, et al. A snake robot for locomotion in a pipe using trapezium-like travelling wave. Mechanism and Machine Theory 2021;158:104221. https://doi.org/10.1016/j.mechmachtheory.2020.104221.

[55] Wright C, Johnson A, Peck A, McCord Z, Naaktgeboren A, Gianfortoni P, et al. Design of a Modular Snake Robot. Proceedings of the 2007 IEEE/RSJ International Conference on Intelligent Robots and Systems, 2007, p. 2609–14.

[56] Wright C, Buchan A, Brown B, Geist J, Schwerin M, Rollinson D, et al. Design and Architecture of the Unified Modular Snake Robot. IEEE International Conference on Robotics and Automation 2012.

[57] Marín Arciniegas JJ, Vivas Albán OA, Marín Arciniegas JJ, Vivas Albán OA. Design and Construction of a Snake-Like Robot Implementing Rectilinear and Sidewinding Gait Motions. TecnoLógicas 2023;26. https://doi.org/10.22430/22565337.2412.

[58] Burdick JW, Radford J, Chirikjian GS. A "sidewinding" locomotion gait for hyper-redundant robots. Proceedings IEEE International Conference on Robotics and Automation, IEEE Comput. Soc. Press; 1993, p. 101–6. https://doi.org/10.1109/ROBOT.1993.291864.

[59] Marvi H, Gong C, Gravish N, Astley H, Travers M, Hatton RL, et al. Sidewinding with minimal slip: snake and robot ascent of sandy slopes. Science (New York, NY) 2014;346:224–9. https://doi.org/10.1126/science.1255718.

[60] Astley HC, Gong C, Dai J, Travers M, Serrano MM, Vela PA, et al. Modulation of orthogonal body waves enables high maneuverability in sidewinding locomotion. Proceedings of the National Academy of Sciences of the United States of America 2015;112. https://doi.org/10.1073/pnas.1418965112.

[61] Kano T, Yoshizawa R, Ishiguro A. TEGOTAE-based control scheme for snake-like robots that enables scaffold-based locomotion. Lecture Notes in Computer Science (including subseries Lecture Notes in Artificial Intelligence and Lecture Notes in Bioinformatics), vol. 9793, Springer Verlag; 2016, p. 454–8. https://doi.org/10.1007/978-3-319-42417-0_46.

[62] Yoshizawa R, Kano T, Ishiguro A. Realization of Snakes' Concertina Locomotion by Using "TEGOTAE-Based Control," Springer, Cham; 2016, p. 548–51. https://doi.org/10.1007/978-3-319-42417-0_61.

[63] Astley HC. Traversing Tight Tunnels—Implementing an Adaptive Concertina Gait in a Biomimetic Snake Robot. Earth and Space 2018, 16th Biennial International Conference on Engineering, Science, Construction, and Operations in Challenging Environments, Reston, VA: American Society of Civil Engineers; 2018, p. 158–68. https://doi.org/10.1061/9780784481899.017.

[64] Bennett AF. Energetics and locomotion. In: Hildebrand M, Bramble DM, Liem KF, Wake DB, editors. Functional Vertebrate Morphology, Cambridge: The Belknap Press of Harvard University; 1985, p. 173–84.

[65] Cao J, Liang W, Wang Y, Lee HP, Zhu J, Ren Q. Control of a Soft Inchworm Robot With Environment Adaptation. IEEE Transactions on Industrial Electronics 2020;67:3809–18. https://doi.org/10.1109/TIE.2019.2914619.

[66] Jurestovsky DJ, Usher LU, Astley HC. Generation of Propulsive Force via Vertical Undulations in Snakes. Journal of Experimental Biology 2021.